LOCAL BUCKLING STUDY OF FLANGES AND WEBS IN I-SHAPES AT ELEVATED TEMPERATURES

Serdar Selamet [1] and Maria E. Garlock [2]

[1] Graduate Student, Department of Civil and Environmental Engineering, Engineering Quad, Room E209A, Princeton University, Princeton, NJ 08544 U.S.A.; Phone: +1-609-258-5437, Fax: +1-609-258-1563; email:sselamet@princeton.edu
[2] Assistant Professor, Department of Civil and Environmental Engineering, Princeton University, Engineering Quad, Room E209A, Princeton University, Princeton, NJ 08544 U.S.A.; Phone: +1-609-258-2728, Fax: +1-609-258-1563; email:mgarlock@princeton.edu

Abstract:

Local buckling in floor beams has been one of the important observations in several fire events in steel buildings such as World Trade Center Tower 7 and large-scale fire experiments such as Cardington in UK. Utilizing three dimensional finite element methods for complex geometry and nonlinear behavior of such connections, local buckling of the web followed by the buckling of the lower flange is observed to occur in early stages in fire, which causes instability to the floor system, and a reduction in the connection strength. To fully capture the behavior of floor systems, one needs to be able to predict such buckling behavior of the beam. This paper contributes to such knowledge by investigating the local buckling of floor beams at elevated temperatures using nonlinear finite element models. The results are compared to AISC provisions of plate buckling under ambient and elevated temperatures.

I - Introduction

Recent experimental and finite element (FE) observations [Moore 2003; Garlock and Selamet 2010] show that local buckling of a floor beam in the vicinity of the connection greatly reduces the axial capacity of the beam during both the heating and the cooling period in a natural fire. During the heating phase, the beam is under compression and the axial forces increase until the lower flange buckles at which point the compressive forces decrease. The deformations caused by the buckling near the connection reduce the tensile capacity of the connection [Selamet and Garlock 2010]. Therefore local buckling controls the maximum compressive and tensile force that a beam experiences in a fire.

The aim of this paper is to investigate the strength of wide flange beams considering local buckling under fire conditions. Previous research on local buckling of steel members focused on isolated plate buckling studies without consideration of the flange (an "unstiffened plate") and the web (a "stiffened plate") interacting with each

other [Karman 1937; Kalyanaraman 1977; Quiel and Garlock 2010]. In this paper we examine the ultimate buckling strength of the flange and webs of I-shapes as they interact with one another. We do this through nonlinear finite element modeling.

II - Description of the finite element model

Our finite element models are created in ABAQUS, a widely used commercial finite element software, using linear, finite membrane strain, fully integrated, quadrilateral shell elements (S4) with 9 integration points (2x2x9) through the thickness. Simpson's integration rule is adopted to extrapolate the stress and strain values at integration points to the nodes on the shell surface. Since a wide range of width-to-thickness ratios are tested under uniform compression, it is necessary to take account both thin and thick shell formulation. Thick shells consider transverse shear deformation and do not assume the Kirchhoff constraint, which states that the plate section through the shell thickness remains normal to the longitudinal axis. As a rule of thumb, a slenderness ratio (*b/t*) larger than 1/15 could develop significant transverse shear deformation [Simulia, 2008]. The Steel Construction Manual [AISC, 2005] offers a wide variety of wide flange sections, some of which have a slenderness ratio larger than 1/15. We are aware that a plate section with a low slenderness ratio will likely yield before it will buckle; nevertheless, due to a significant decrease in rigidity (elastic modulus) of the shell cross section at elevated temperatures, a formulation with thick shell consideration is selected to capture an accurate behavior of such plates.

Table 1: Material properties at ambient and elevated temperatures for S275 Grade Steel according to Eurocode

Temperature	$k_p(T)$	$k_y(T)$	$k_e(T)$	$F_y(T)$ in MPa	$F_u(T)$ in MPa	$E(T)$ in GPa
20	1	1	1	303.0	469.6	207.0
100	1	1	1	303.0	469.6	207.0
200	0.807	1	0.900	303.0	469.6	186.3
300	0.613	1	0.800	303.0	378.7	165.6
400	0.420	1	0.700	303.0	303.0	144.9
500	0.360	0.780	0.600	236.3	236.3	124.2
600	0.180	0.470	0.310	142.4	142.4	64.2
700	0.075	0.230	0.130	69.7	69.7	26.9
800	0.050	0.110	0.090	33.3	33.3	18.6
900	0.038	0.060	0.068	18.2	18.2	13.9

The material properties of I-shaped cross sections are taken from previously studied research [Garlock and Selamet 2010] as shown in Table 1. The parameters k_p, k_y and k_e represent the proportional stress, yield stress and elastic modulus reduction factors, respectively [ECCS 2001]. The yield and ultimate stress of the material is denoted as $F_y(T)$ and $F_u(T)$, respectively. $E(T)$ is the modulus of elasticity at the given temperature (equal to E at ambient temperature times k_e) The steel material is modeled with 'von Mises' plastic flow and isotropic strain hardening. No material softening is included as this would greatly decrease the convergence character of the

problem. The steel material behavior at elevated temperatures is adopted from Eurocode 3 provisions [Eurocode 2001].

Some of the simulations that we have done represent the *isolated* plates for different boundary conditions (as described in the Section III) and some represent flanges and webs in an I-shaped *assembly* (as described in the Section V). For all models, the loaded edges are simply supported. The boundaries of unloaded edges of isolated plates are simply supported or fixed (from rotation and vertical translation) or free in all degrees of freedom.

III - Mesh convergence and critical buckling study of isolated plates

To properly represent buckling using the finite element method one must represent a continuous plate section using smaller quadrilateral elements. A coarse meshing of the section will yield unconservative results in the buckling strength of the plate. Having a very fine mesh will be computationally inefficient and it might create numerical convergence issues near the bifurcation load. Eurocode 3 suggests meshing at least 6 shell elements in the expected half wavelength of the buckling shape [JRC, ECCS 2007]. The most effective way to check mesh convergence is to run several eigenvalue extraction analyses with different mesh densities. Comparing the first couple of eigenvalues to the theoretical eigenvalues will indicate if the finite element mesh is fine enough. The eigenvalue extraction analyses are very fast as opposed to the costly load displacement (static or dynamic) analyses.

The lowest eigenshapes (buckling shape) of the stiffened isolated plates with simply supported (Case 1) and fixed (Case 2) unloaded edges are shown in Table 2. It is seen that Case 1 has 5 half waves (i.e. n=5) and Case 2 has 8 half waves. Similarly, the buckling shapes of the unstiffened isolated plates with simply supported (Case 3) and fixed (Case 4) unloaded edges are illustrated in Table 2 with 1 and 3 half waves, respectively. The mesh density of isolated plates is also used for plates in I-shaped cross sections. The critical buckling stress, F_{cr}, is theoretically equal to:

$$F_{cr} = \frac{k\,E\,\pi^2}{12\,(1-v^2)\,(b/t)^2} \qquad \text{Eq. (1)}$$

$$k = (n/\alpha)^2 + p + q\,(\alpha/n)^2 \qquad \text{Eq. (2)}$$

where v is the poisson's ratio, b is the plate width, t is the plate thickness and k is the buckling coefficient which represents the boundary condition. The buckling coefficient k is found by using Equation 2 derived by Bleich [1952]. His equations represent not only simply supported or fixed boundary conditions but various restraints in between, which are denoted by the parameters p and q. The aspect ratio and the number of half waves across the plate length are denoted by α and n, respectively.

The values from Equation 2 for all four cases are shown in Table 2. It is important to note that the Steel Construction Manual [AISC, 2005] suggests that the buckling coefficient k is 4.0 and 0.425 for Case 1 and Case 3, respectively. The buckling coefficient 4.0 is an accurate estimate for Case 1 with the aspect ratio α equal to 5 according to the elastic plate buckling theory. However, the value 0.425 is conservative for Case 3 with α=5. A rigorous analysis on the general plate buckling coefficient formulation [Bleich, 1952] reveals that $\alpha \geq 50$ is needed to converge to $k = 0.425$. To keep the mesh convergence study accurate, the theoretical buckling coefficient k is taken as 0.465 using the Equation 2 with $\alpha = 5$.

Table 2: Buckling coefficient for web (stiffened) and flange (unstiffened) isolated plates for both simply supported and fixed boundary conditions on unloaded edges.
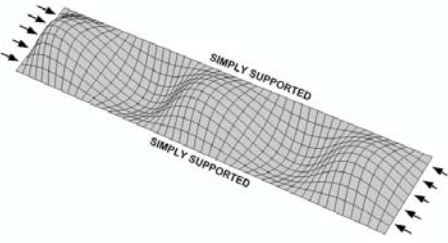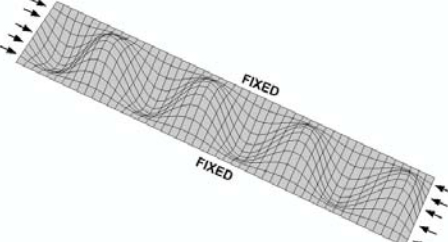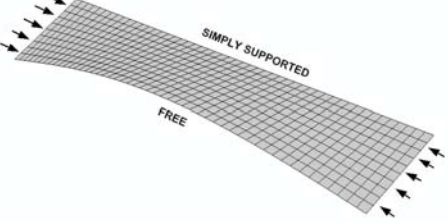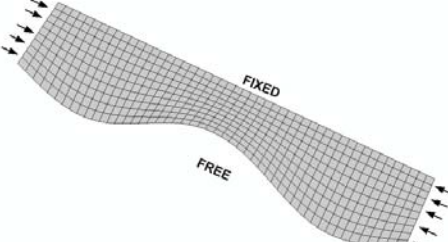
		Boundary Conditions	Parameters
STIFFENED (WEB)	**Case 1**		**k = 4.0** *α=5; n=5* *p=2; q=1*
	Case 2		**k = 7.01** *α=5;n=8* *p=2.5;q=5*
UNSTIFFENED (FLANGE)	**Case 3**		**k = 0.465** *α=5;n=1* *p=0.425;q=0*
	Case 4		**k=1.277** *α=5;n=3* *p=0.57;q=0.125*

Table 3: Results for the 1st eigenvalue value analyses of isolated webs and flanges for various *b/t* ratios.

	F_{cr} (MPa)							
	WEB				**FLANGE**			
	Case 1		**Case 2**		**Case 3**		**Case 4**	
	(5 half waves)		(7 or 8 half waves)		(1 half wave)		(3 half waves)	
b/t	**FE**	**theory**	**FE**	**theory**	**FE**	**theory**	**FE**	**theory**
10	7175	7483	11482	13114	844.4	869.9	2288	2389
16	2899	2923	4938	5123	334.1	339.8	917.0	933.2
20	1870	1870	3238	3279	214.8	217.5	591.0	597.3
25	1203	1197	2105	2098	137.9	139.2	380.1	382.3
33	679.4	687.2	1199	1204	77.8	79.9	214.7	219.4
40	472.6	467.7	837.4	819.7	54.1	54.4	149.4	149.3
50	302.8	299.3	538.1	524.6	34.7	34.8	95.8	95.6
57	232.0	230.3	412.8	403.6	26.5	26.8	73.4	73.5
65	179.7	177.1	320.0	310.4	20.6	20.6	56.8	56.5
77	128.1	126.2	228.4	221.2	14.7	14.7	40.5	40.3
87	100.3	98.9	178.8	173.3	11.5	11.5	31.7	31.6
100	75.8	74.8	135.3	131.1	8.7	8.6	24.0	23.9

Table 3 shows values of F_{cr} for the boundary conditions shown in Table 1 and various slenderness ratios *b/t*. The tested plate has the following properties: *E*=207 GPa, *v*=0.3 and *b/t*=87. Both the theoretical (theory) values (based on Equations 1 and 2) and the finite element (FE) results (based on an eigenvalue analysis) are shown. It is important to mention that the buckling shape corresponding to the lowest (1st) eigenvalue is different for each case, which is denoted as the number of half waves across the plate length. FE results essentially equal the theoretical solutions. For the plate simply supported or fixed along the unloaded edges (Cases 1 and 2: web), the *b/10* element size converges to the theoretical value within 4%. For the plate simply supported or fixed on one unloaded edge and free on the other edge (Cases 3 and 4: flange), the *b/10* mesh element size approaches to the theoretical value also within 3%.

The largest percent difference from theoretical buckling strength is for the slenderness ratio *b/t*=10 as expected because *b/t*=10 belongs to a thick shell category and theoretical values assume a thin shell formulation. The mesh size equal to *b/10* is used for plates in static load displacement analyses since it gives an accurate prediction of the elastic buckling theory.

IV - Imperfection study

The effect of the imperfection magnitude of the first (lowest) buckling shape on the buckling strength of the plates representing the isolated web and flange sections has been studied previously [e.g., Quiel and Garlock 2010]. In that study, two imperfection magnitudes were tested where the peak of the sinusoidal wave imperfection equals to *b/200* or to 10% of the plate thickness (*0.1t*). A parametric study with several slenderness (*b/t*) ratios was conducted by changing the shell

thickness and keeping the plate width and length (*b* and *a*) constant. This method avoids re-meshing the plate for each different *b/t*. Since the plate width *b* stays constant, the first imperfection method (*b/200*) applies the same imperfection magnitude from compact to very slender elements. The second method (*0.1t*), however, changes the imperfection magnitude for each different *b/t* ratio. The difficulty is that for very slender plate sections tested in the parametric study, *b/200* could lead to almost 50% of the plate thickness which is a large initial imperfection.

In this study we use initial imperfections corresponding to the lowest eigenvalues (see Table 2) and apply them to the load-displacement analyses by scaling the buckling shapes such that the maximum deflection in the models is *0.1%* of the plate thickness. Figure 1 compares the buckling strength of slender and not-slender web and flange sections as a function of the initial imperfection magnitude. It is seen that slender web sections are not imperfection sensitive whereas not so slender (closer to compact) web sections are rather imperfection sensitive and their buckling strength could drop as much as 30% if the imperfection magnitude equals the plate thickness. Both slender and not-slender flange sections, which already have a much smaller buckling strength, are not sensitive to imperfections.
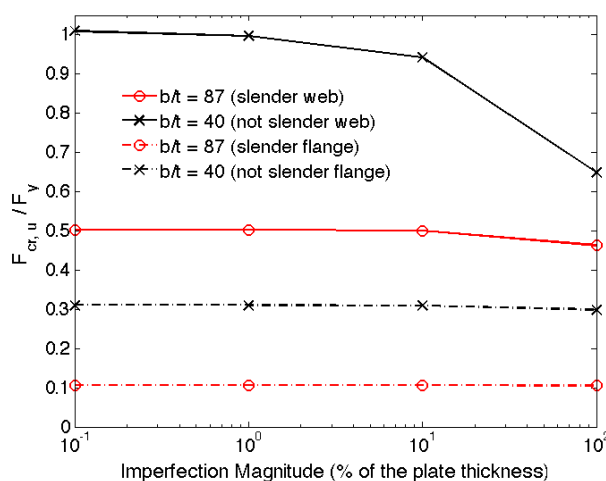

Figure 1: The buckling strength F_{cr}/F_y of both isolated web and flange sections at ambient temperature with maximum imperfection magnitude on the log-scale x axis

Geometric imperfections and residual stresses must be taken account in buckling design criteria. Intensive theoretical and empirical research has been completed since 1950's on both imperfections and residual stresses [Galambos 1988; AISC 2005]. Since the magnitude and the shape of the imperfections in a structure cannot be known apriori, we conducted finite element buckling studies with a very small imperfection magnitude (*0.1%*t*) and no residual stresses. The purpose is to see the ideal behavior of plates without significant effects of imperfection. The AISC design curve, which includes the effects of both imperfection and residual stresses, is expected to be conservative compared to our finite element results.

V- Ultimate buckling capacity of isolated plates and I-shaped sections

Until now our studies have focused on the critical buckling capacity (F_{cr}) of isolated plates based on eigenvalue analyses or elastic theory (Equation 1). Now we examine the ultimate (i.e., post-buckling) capacity ($F_{cr,u}$) of plates in I-shaped sections as shown in Figure 2 and compare them to $F_{cr,u}$ of isolated plates. $F_{cr,u}$ is found by dividing the total nodal forces applied to the isolated plate or I-shaped section and dividing it by the area where the forces are applied. $F_{cr,u}$ corresponds to the average stress in the section when the field equations of the models stop converging.

Cases 5, 6, and 7, shown in Figure 2 have different loadings on an I-beam, which come close to representing how that beam is loaded depending on the connections. For example, in Case 5, only the web section is uniformly loaded and it represents the loading scenario for simple shear connections in a fire. In Case 6, only the flange sections are uniformly loaded and it may represent a connection such as a top-and-seat angle where the web is not connected. Also, our previous studies (Garlock and Selamet 2010, Selamet and Garlock 2010) show that once the beam rotates sufficiently early in a fire, the bottom flange contacts the supporting member and subsequently the bottom flange is loaded in compression until it buckles. Therefore, Case 6 also represents simple shear connections. In Case 7, the entire section is uniformly loaded. This case represents some common moment connections where both the flanges and web are connected.
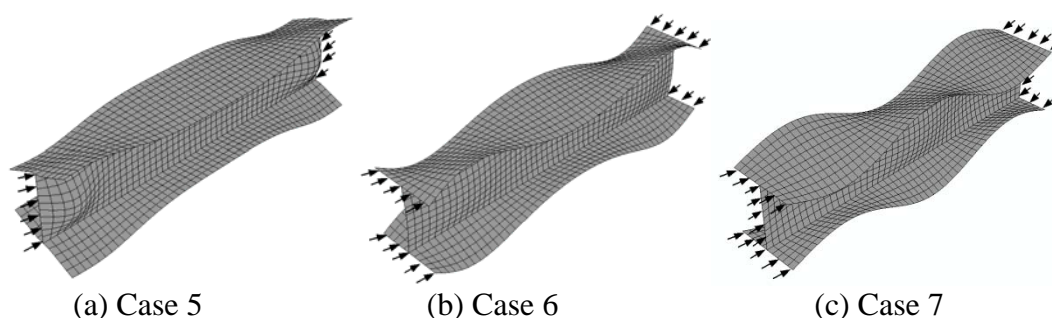

(a) Case 5 (b) Case 6 (c) Case 7

Figure 2: The buckling shape of the lowest eigenvalue for I-shape cross section composed of *b/t*=50 flange and *b/t*=100 web under uniformly loaded (a) web only (Case 5), (b) flanges only (Case 6) and (c) entire cross section (Case 7).

Furthermore, this study permits a comparison of the isolated plate study, where Cases 1 and 2 (stiffened plate) can be compared to Cases 5 and 7, and similarly, Cases 3 and 4 (unstiffened plates) can be compared to Cases 6 and 7. The isolated buckling study assumes either a simply supported (Case 1 or 3) or fixed (Case 2 or 4) boundary condition. In reality, the flange or web is neither fully restrained nor it is fully free to rotate at the edge where it connects to another plate (web or flange). The rotational restraint depends on the stiffness of the connecting plates. Several approximate analytical solutions have been derived [Bleich, 1952]; however these equations are

tedious to solve and have significant assumptions. The finite element method provides an alternative way to estimate the buckling strength of plates in an assembly.

To estimate $F_{cr,u}$, the same method is used for both plates in an assembly and isolated plates. First, the theoretical buckling capacity F_{cr} and the buckling shape are estimated from the models by using the eigenvalue extraction method. An initial imperfection is introduced in the model (as explained in Section IV), then a static load-displacement analysis is run to determine $F_{cr,u}$. For buckling studies using this method, the load increment must be small to capture the same buckling shape that is introduced by the initial imperfection. At the bifurcation load, a large load increment could introduce a different buckling shape (with a higher eigenvalue; e.g. higher buckling strength) that does not represent the initial imperfection, which defeats the purpose of such initial imperfection. Hence, the user must check if every analysis is failed by the introduced buckling shape.

Figure 3 compares the buckling stress $F_{cr,u}$ of <u>web</u> plates in an assembly (Cases 5 and 7a) to that predicted by isolated stiffened plates (Cases 1 and 2). Case 7a (loading Case 7 in Fig 2) keeps the flange b/t value constant (either slender or stiff as defined below) but varies the web b/t. $F_{cr,u}$ is normalized to the yield stress (F_y) in the plots. For some values, $F_{cr,u}/F_y$ values are greater than 1 since strain hardening is used in material properties (see Table 1). The response at various temperatures is examined: 100°C, 400°C, 600°C and 900°C. The web in beam sections (Case 5) is either connected to very slender flanges (*b/t*=50) or to stiff flanges (*b/t*=5). This variation allows one to observe differences in $F_{cr,u}$ of the web with a small or large rotational restraint at the boundaries.

Figure 3 shows that at ambient temperature (Figure 5a) there are differences between the isolated plate behavior and the plate assembly behavior, where the web in the assembly (Case 5) is stronger than the isolated plate response. The reason for this is that the flanges provide axial restraint, which stiffens the boundary conditions. It is also seen that the flange slenderness (stiff versus slender) has a significant effect on the buckling strength. Further, the results for isolated web plate with simply supported edges (Case 1) closely match those of Case 5 with slender flanges for temperatures T ≥ 400 °C. The same is true for web plates with fixed edges compared to Case 5 with stiff flanges for temperatures T ≥ 400 °C. When the entire section is loaded, Case 7a with stiff flanges closely follows Case 2 (isolated web with fixed boundaries) for all temperatures. This is expected since stiff flanges provide an almost full rotational rigidity. However Case 7a with slender flanges has almost no strength at all since the flanges buckle right away destabilizing the entire cross-section.
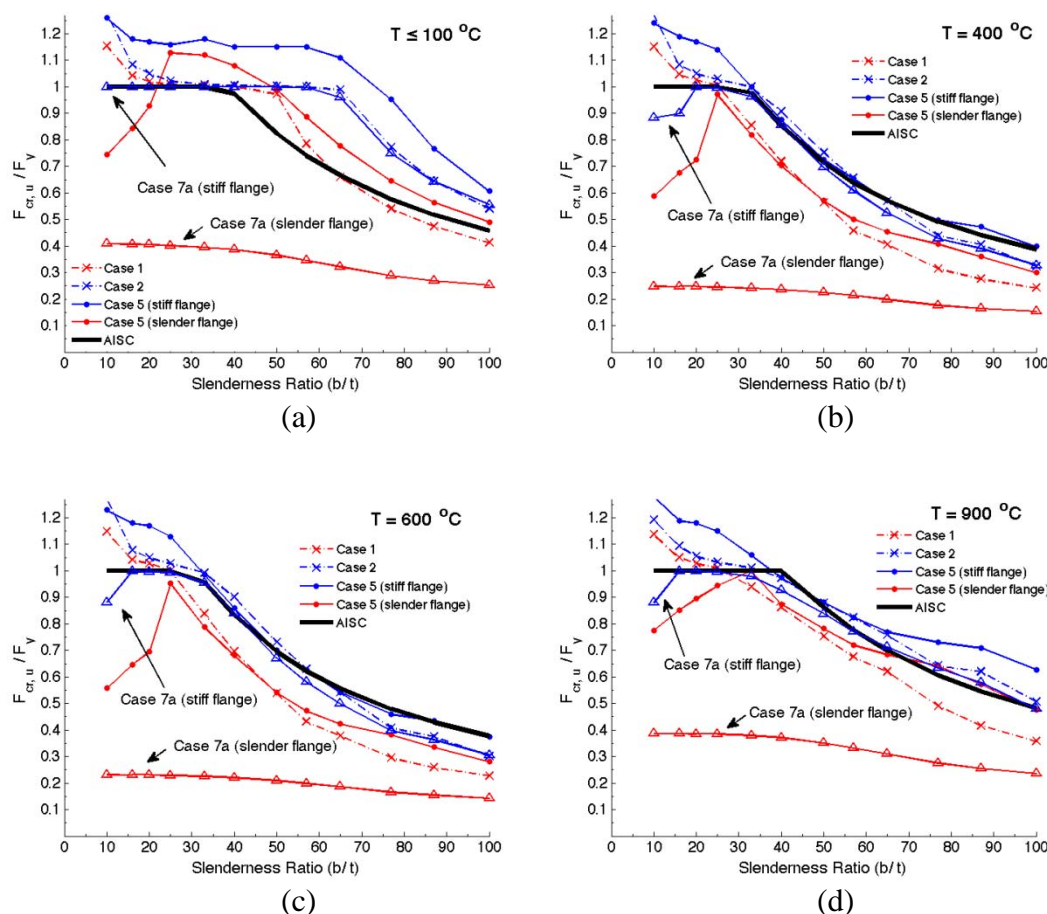
Figure 3: Normalized $F_{cr,\,u}$ for isolated and I-beam <u>web</u> sections with several boundary conditions are compared to AISC design curve for stiffened plates at temperatures (a) T $\leq 100°$C, (b) T $= 400°$C, (c) T $= 600°$C and (d) T $= 900°$C.

For webs in I-shaped sections, there is not only rotational restraint but, as mentioned before, also translational (axial) restraint provided by the adjacent flanges since only the web section is loaded as opposed to the entire I-shape cross section. This type of loading causes contraction in the web section which is resisted by the connecting flanges and ultimately results in greater buckling strength of the web section. If the flanges in these web-loaded analyses are slender, the axial force that is transferred to them causes them to buckle before the web. This happens with webs that are stiff ($b/t \leq 25$), and what results is a significant drop in $F_{cr,u}$ as seen in Figure 3.

Figure 3 also plots the AISC design curve for stiffened plates based on the Steel Construction Manual [AISC, 2005] using Eqn E7-17 (where $b_e/b = F_{cr}/F_y$, see Quiel and Garlock 2010). The AISC solution is independent of the flange slenderness so that the AISC comparison can be made for all cases (Case 1, 2, and both Case 5 with slender and stiff flanges). At temperatures T $\leq$ 100 °C, AISC design curve is conservative. However, as the temperature increases, AISC becomes unconservative for Case 1 and Case 5 with slender flanges. AISC design curve is generally closer to the solution of isolated web with fixed edges (Case 2) and Case 5 with stiff flanges.
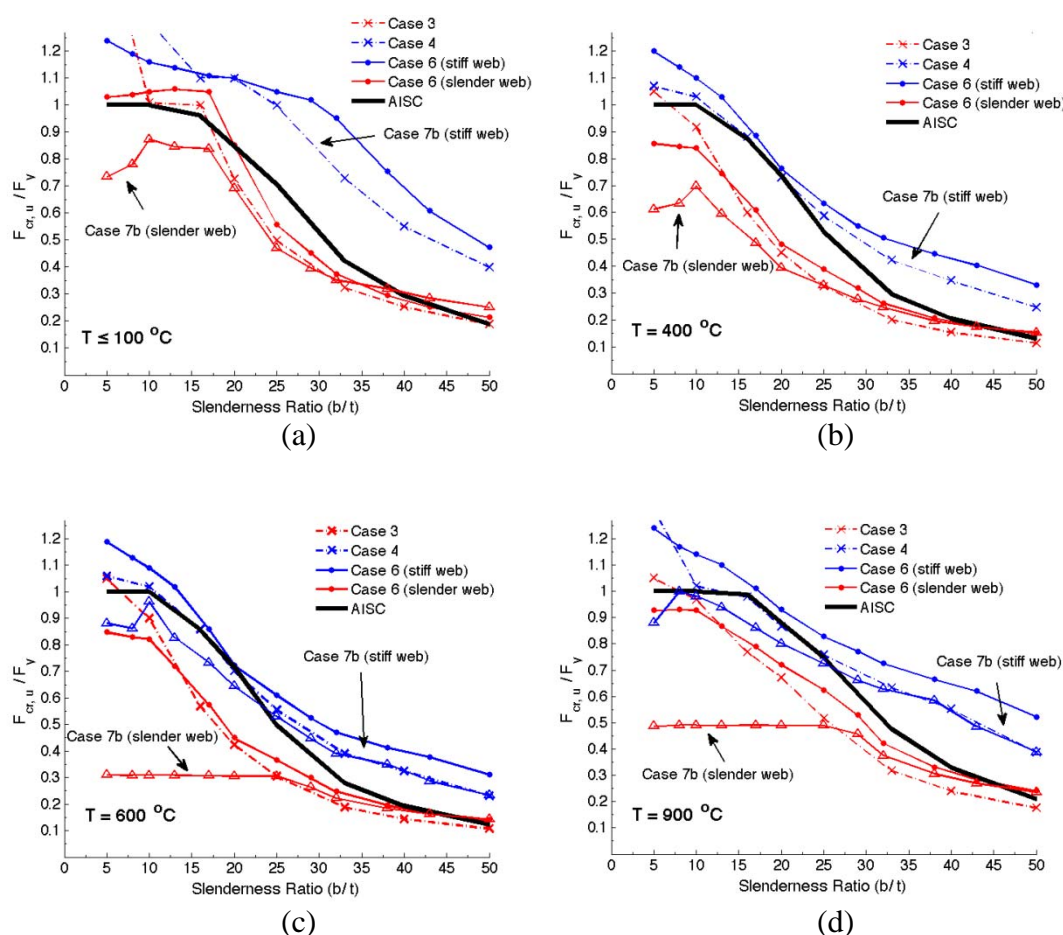
Figure 4: Normalized $F_{cr,u}$ for isolated and I-beam <u>flange</u> sections with several boundary conditions are compared to AISC design curve for unstiffened plates at temperatures (a) T $\leq 100°$C, (b) T = 400°C, (c) T = 600°C and (d) T = 900°C.

Figure 4 compares $F_{cr,u}/F_y$ of <u>flange</u> plates in an assembly (Cases 6 and 7b) to that predicted by isolated unstiffened plates (Cases 3 and 4). Case 7b (loading Case 7 in Fig 2) keeps the web b/t value constant (either slender or stiff as defined below) but varies the flange b/t. The flanges in beam sections (Case 6) are either connected to a very slender web (b/t=100) or to a stiff web (b/t=10). The results for Case 3 and Case 6 with slender web sections agree well for all temperatures. Case 6 with slender web sections have greater buckling strength than Case 3 for all slenderness ratios except for $b/t \leq 10$. For $b/t \leq 10$, the slender web section which provides restraint for the flanges buckles first. This causes a drop in $F_{cr,u}$ but it is not as pronounced as for Case 5 with slender flange sections (see Figure 3). The results for Case 6 are always greater than those for isolated plates (Case 3 and 4). This is due to the translational (axial) resistance provided by the stiff web to the flanges. The difference in $F_{cr,u}$ for stiff or slender (fixed or simply supported) restraint is more pronounced for flanges (Fig. 4), than for webs (Fig. 3). For all temperatures, Case 7b with a stiff web exactly matches Case 4 (isolated flanges with fixed boundaries) so it looks like only one line is plotted. This is expected since stiff flanges provide an almost full rotational rigidity.

Case 7b with a slender web closely follows Case 3 (isolated flange with fixed boundaries) for all temperatures but only for larger flange b/t ratios. For flanges with a low *b/t*, the slender web buckles first and hence reduces the $F_{cr,u}$ of the I-shape.

Figure 4 also plots the AISC design curve for unstiffened plates based on the Steel Construction Manual [AISC, 2005] using Equations E7-4 through E7-6 (where F_{cr}/F_y = Q_sF_y). Like the web study described previously, the AISC solution is independent of the web slenderness so that the AISC comparison can be made for all cases (Case 3, 4, and both Case 6 with a slender and a stiff web). At temperatures $T \leq 100$ °C, AISC design curve is in between Case 3 and Case 4, but closer to Case 3. This is expected since AISC design curve assumes that the isolated flange sections are neither simply supported nor fixed but somewhere in between. As the temperature increases, AISC gets closer to the buckling performance of Case 4 and Case 5 with a stiff web for $b/t \leq 30$.

VI - Conclusion

In this paper, the post-buckling strength webs and flanges in a beam under fire conditions is investigated. The finite element models are validated against theoretical buckling strength of plates. Two types of models were created: (1) *isolated* plates with idealized simply supported or fixed boundary conditions, and (2) plates *assembled* to form an *I-shape*. Several load case I-shape models were created to represent different connections. For example, the I-shape model with only the web axially loaded represented a simple shear connection design, the I-shape model with only the flanges axially loaded represented a top-and-seat connection design, and the model with the entire I-shape loaded represents a moment connection with a web connection component.

Results of our study show the following:
- Estimating the post-buckling capacity ($F_{cr,u}$) of a web or flange with isolated plates typically results in $F_{cr,u}$ *less than* the results of a model with an I-shape assembly where only the flange or web is loaded. The reason for this phenomenon is that, for example, if the web is loaded, some of the axial force is transferred to the flanges and the flanges provide axial restraint.
- As the temperature in the plate increases, the isolated plate solution for $F_{cr,u}$ develops better correlation to that based on the I-shape model.
- The stiffness of the connecting element has a significant influence on $F_{cr,u}$. For example, if a web is connected to a stiff flange, or a flange is connected to a stiff web, the $F_{cr,u}$ is larger than if these elements were connected to more slender elements. This effect of the connecting element stiffness on $F_{cr,u}$ is more pronounced in flanges with axial loads than in webs.
- In general, there is not too much of a difference in the results for loading the entire cross section versus loading components of it (unless the flange or web are too slender)

- The AISC design prediction for post-buckling strength of slender plates is generally unconservative for elevated temperatures, especially for plates connected to slender elements.

Our goal as this research progresses is to develop predictive equations that determine when a beam flange or web will buckle during a fire. Since flange buckling marks the point of maximum compression force in the beam, it is important to be able to determine that force for developing a performance-based approach for fire safety.

VIII - References

[1] AISC (2005). "*Load and Resistance Factor Design, 13th Edition*".
[2] Becque, J. and Rasmussen, J. R. (2009). "Numerical Investigation of the Interaction of Local and Overall Buckling of Stainless Steel I-Columns", Journal of Structural Engineering, ASCE, 65(8-9), pp. 1349-1356.
[3] Bleich, F. (1952). "Buckling Strength of Metal Structures", *Engineering Societies Monographs*, McGraw Hill, New York
[4] European Committee for Standardization -ECCS (2001). "*Eurocode 3: Design of steel structures Part 1.2: General Rules Structural fire design ENV 1993-1-2:2001*".
[5] European Committee for Standardization - ECCS (2004). "*Eurocode 3: Design of Steel Structures Part 1-5 Plated Structural Elements*".
[6] European Committee for Standardization - ECCS Technical Committee 8 Structural Stability (2008). "*Buckling of Steel Shells European Design Recommendations, Eurocode 3, Part 1-6*", 5th Edition.
[7] Galambos, T. V. (1988). "*Guide to Stability Design Criteria for Metal Structures*", 4th Edition, John Wiley & Sons, New York.
[8] Garlock, M. and Selamet S. (accepted in 2010). "Modeling and Behavior of Steel Plate Connections Subject to Various Fire Scenarios", *Journal of Structural Engineering*.
[9] Kalyanaraman, V., Pekoz, T., and Winter, G. (1977). "Unstiffened Compression Elements", *Journal of the Structural Division*.
[10] Karman, T. V., Sechler, Ernest, E. and Donnell, L. H. (1937). "The Strength of Thin Plates in Compression", *Trans. ASME*, 54. APM 54–5.
[11] Maljaars, J., Soetens, F., and Snijder, H. H. (2009). "Local buckling of aluminium structures exposed to fire Part 2: Finite element models", *Thin-Walled Structures*, 47, 1418-1428.
[12] Quiel, S. E., and Garlock, M. E. M. (2010). "Calculating the Buckling Strength of Steel Plates Exposed to Fire", tentatively accepted for publication in *Thin-Walled Structures*.
[13] Rhodes, J. (1982) "Effective widths in plate buckling". In: J. Rhodes and A.C. Walker, Editors, *Developments in Thin-Walled Structures—1*, Applied Science Publishing, London, pp. 119–158.
[14] Scientific and Technical Reports - JRC and European Committee for Standardization - ECCS (2007). "*Commentary and Worked Examples to EN 1993-1-5 Plated Structural Elements*".
[15] Selamet, S., and Garlock, M. (submitted in 2010). "Robust Fire Design of Single Plate Shear Connections", *Engineering Structures*.
[16] Simulia (2008). "*Abaqus Documentation version 6.8*".
[17] Vinnacota, R. (2005). "*Steel Structures: Behavior and LRFD*".